Design and Development of an Experimental Setup of Electrically Powered Spinning Rotor Blades in Icing Wind Tunnel and Preliminary Testing with Surface Coatings as Hybrid Protection Solution

Eric Villeneuve *,† , **Caroline Blackburn** † **and Christophe Volat**

Anti-icing Materials International Laboratory (AMIL), Department of Applied Sciences,
Université du Québec à Chicoutimi (UQAC), 555 Boulevard de l'Université, Chicoutimi, QC G7H2B1, Canada;
caroline_blackburn@uqac.ca (C.B.); christophe_volat@uqac.ca (C.V.)
* Correspondence: eric1_villeneuve@uqac.ca
† These authors contributed equally to this work.

Abstract: In order to study ice protection systems for rotating blades, a new experimental setup has been developed at the Anti-Icing Materials International Laboratory (AMIL). This system consists of two small-scale rotating blades in a refrigerated icing wind tunnel where atmospheric icing can be simulated. Power is brought to the blades through a slip ring, through which the signals of the different sensors that are installed on the blades also pass. As demonstrated by the literature review, this new setup will address the need of small-scale wind tunnel testing on electrically powered rotating blades. To test the newly designed apparatus, preliminary experimentation is done on a hybrid ice protection system. Electrothermal protection is combined with different surface coatings to measure the impact of those coatings on the power consumption of the system. In anti-icing mode, the coatings tested did not reduce the power consumption on the system required to prevent ice from accumulating on the leading edge. The coatings however, due to their hydrophobic/superhydrophobic nature, reduced the power required to prevent runback ice accumulation when the leading edge was protected. One of the coatings did not allow any runback accumulation, limiting the power to protect the whole blades to the power required to protect solely the leading edge, resulting in a potential 40% power reduction for the power consumption of the system. In de-icing mode, the results with all the substrates tested showed similar power to achieve ice shedding from the blade. Since the coatings tested have a low icephobicity, it would be interesting to perform additional testing with icephobic coatings. Also, a small unheated zone at the root of the blade prevented complete ice shedding from the blade. A small part of the ice layer was left on the blade after testing, meaning that a cohesive break had to occur within the ice layer, and therefore impacting the results. Improvements to the setup will be done to remedy the situation. Those preliminary testing performed with the newly developed test setup have demonstrated the potential of this new device which will now allow, among other things, to measure heat transfer, force magnitudes, ice nucleation, and thermal equilibrium during ice accretion, with different innovative thermal protection systems (conductive coating, carbon nanotubes, impulse, etc.) as well as mechanical systems. The next step, following the improvements, is to measure forced convection on a thermal ice protection system with and without precipitation and to test mechanical ice protection systems.

Keywords: icing; wind tunnel; experimental testing; aerospace; hydrophobic; superhydrophobic; icephobic; coatings; ice protection system; rotorcraft

1. Introduction

Many structures are affected by atmospheric icing—such as airplanes, boats, wind turbines, transmission lines, and helicopters. Rotorcrafts are vulnerable to in-flight and preflight icing, which considerably limits their operation. The most adverse effects come from

the aerodynamics of the iced rotor blades, resulting in drag increases and flow separation which severely affect lift forces and make control very difficult. Asymmetric ice shedding also induces severe vibrations that can force emergency landings. Although the primary concern is with the main rotor, protection of the tail rotor requires similar considerations. Even if the capability of operating rotorcraft under icy conditions [1] is considered a priority, de-icing and anti-icing remain a largely unfilled aspiration. Currently, only electro-thermal systems consisting of periodically heating the iced leading edge of the blades are in use. Practically, because of the high energy load required for heating as well as the high electrical current flowing in the slip rings and the long cabling required, certified electro-thermal de-icing systems can presently only equip the main rotors of large rotorcraft. Because of the low power available, small helicopters cannot be equipped with an electro-thermal de-icing system, which prohibits them from operating under icy conditions. Deicing costs can be reduced when the most important blade sections are protected, such as the leading edge, and two-thirds of the outer parts of the blade [2]. Passive systems, such as icephobic coatings applied on exposed surfaces, appear to be an interesting solution to prevent ice accumulation or minimize its adherence.

A lot of research and experimentation still needs to be done on ice protection systems for rotorcraft. Several setups have been developed over the past decades to study the icing on rotorcraft blade. The Anti-icing Materials International Laboratory (AMIL) at the Université du Québec à Chicoutimi had previously developed the spinning rotor blade (SRB) to evaluate ice shapes and measure the ice adhesion on different surface coatings applied to scaled-down rotorcraft blade in rotation submitted to representative atmospheric icing [3]. Wang et al. [4] conducted experiments using a rotating blade in a cold chamber, under various icing conditions. The ice shapes, the influence of different icing temperatures, rotation speeds, liquid water content, icing times, number of blades on the rotor and blade material were analyzed. Liu et al. [5] investigated the dynamic ice accretion into an icing wind tunnel on a rotating propeller model. The power consumption measurements revealed that the propeller consumes more power under icing conditions. The National Research Council (NRC) has developed an in-situ rotating ice adhesion rig installed in the Altitude Icing Wind Tunnel (AIWT) [6] to measure the adhesion properties of ice to various icephobic coatings [7]. In this setup, the samples are iced when fixed or at very slow rotation speeds. Once the ice is accreted, the rotation speed is linearly increased until ice is detached. However, no power can be supplied to the blades in rotation with those setups and they cannot be used to test active ice protection systems. Laroche [8] studied the thermal efficiency, and temperature uniformity of three different heating element materials. Tests were performed on flat heater coupons in an icing wind tunnel but not in rotation. Antonini et al. [9] studied the effect of superhydrophobic coatings on surfaces exposed to icing conditions. All tests were performed in an open loop icing wind tunnel on a standard NACA0021 airfoil, fixed, and equipped with an electrical heater mounted on a leading edge. Those setups allow testing of active ice protection systems but are limited to fixed wings only.

Palacios et al. [10,11] presented a novel pneumatic approach to protect helicopter rotor blades from ice accretion. Testing was conducted in the Adverse Environment Rotor Test Stand Facility [12], which is capable of generating icing in a cold room on rotating blades. This test setup allowed Palacios [13] to design, fabricate, and test a low-power, non-thermal, ultrasonic de-icing system as a potential replacement of current electro-thermal systems on helicopter rotor blades. The proposed de-icing actuator system however remained conceptual. While this setup is able to test active protection systems in rotation, it is not installed in a wind tunnel and cannot generate representative atmospheric icing conditions at various wind speed, simulating forward flight. Li [14] by using the Icing Research Tunnel of Iowa State University (ISU-IRT), conducted a series of experimental studies in order to investigate the dynamic ice accretion process on the surface of three different kinds of aero-engine spinner-fan models and to explore the feasibility of different anti-/de-icing technologies. In this study, a superhydrophobic coating was used for icing mitigation and

also the anti-/de-icing performance using a hot air circulating system was evaluated. In this setup, only hot air can be used for active ice protection, no other source of energy can be supplied to the blade.

Huang et al. [15] reviewed the state-of-the art of icephobic coatings for various applications and their efficiency. Despite the promising results obtained with coatings, Huang suggested that they should be considered as a complementary option to either thermal or mechanical ice protection methods. Therefore, following a quick analysis of these assemblies, none of them can be used to test active ice protection systems subjected to atmospheric icing in an icing wind tunnel on rotating blades. None of them can perform testing on hybrid systems, combining active and passive methods, or assess the effectiveness of an icephobic coating combined with thermal heating or another mechanical/active method applied to the leading edge of rotating helicopter blades. To address this need, AMIL has decided to modify its SRB Setup [3] in order to be able to bring electric power to various devices like heating elements, conductive coatings or piezoelectric elements installed on the rotating blades. This new device will now allow, among other things, to measure heat transfer, force magnitudes, ice nucleation, and thermal equilibrium during ice accretion, different innovative thermal protection systems (conductive coating, carbon nanotubes, impulse, etc.), as well as mechanical systems. This paper presents the design and construction of the modified setup as well as the preliminary test campaign performed to validate the efficiency of the resulting system. In this preliminary test campaign, different surface coatings are applied to thermally protected blades in order to measure their impact on the protection of the blades.

2. Experimental Setup

2.1. Refrigerated Wind Tunnel

The Powered-Spinning Rotor Blade (P-SRB) experimental setup was designed for testing in a refrigerated wind tunnel at AMIL. AMIL's icing wind tunnel (IWT), shown in Figure 1, is a closed-loop low speed refrigerated wind tunnel able to operate at subzero temperatures at sea level pressure. The refrigeration system capacity is able to vary the total air temperature between $-48\ ^\circ$C and $22\ ^\circ$C by passing the air through a heat exchanger of 1.6×1.6 m (Figure 2), which is powered by a compressor and a glycol pump (Figure 2).
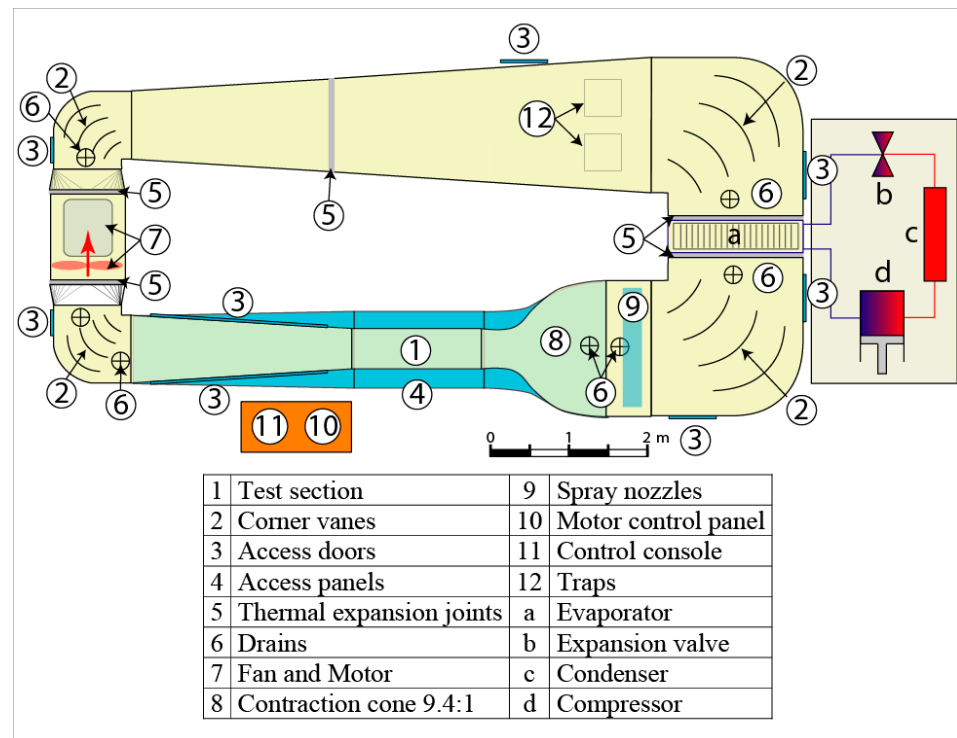

Figure 1. Icing wind tunnel.

Figure 2. Icing wind tunnel schematic [16].

The IWT has two test sections. The larger test section is 0.91 m wide by 0.76 m high and tests can be run at air speeds up to 50 m/s at room temperature. The wind tunnel meets the conditions [17] of the Society of Automotive Engineers (SAE) Aerospace Recommended Practice for icing wind tunnel ARP5905 [18] and Aerospace Information Report for droplet sizing AIR4906 [19]. The IWT test section air speed is controlled by computer via a control program and data acquisition card. The test section air speed is calculated with the Bernoulli equation. The speed in the test section is given by

$$U_{TestSection} = \sqrt{2\left(1 - \frac{A_{TestSection}^2}{A_{RampSection}^2}\right)^{-1} \frac{p_{RampSection} - p_{TestSection}}{\rho_{air}}} \tag{1}$$

where the density of air (ρ_{air}) is calculated from the test air temperature and pressure. This value is considered constant throughout a single test since the temperature and velocity in the tunnel are maintained with very few deviations during a test. A water spray system is used to generate the icing cloud. It is composed of up to three spray ramps of eight to nine air atomizing nozzles composed of pneumatic sprinklers each (Figure 3). The water line is under pressure and rotameters control the flow rate to meet the desired liquid water content while the water droplet diameter is controlled by the air pressure injected into the nozzle. A cooling unit controls the water temperature used to produce a cloud of supercooled water droplets with median volumetric diameters (MVD) ranging from 20 to 100 μm and liquid water contents (LWC) ranging from 0.1 to 3.0 g/m^3. The water is filtered and cleaned to obtain osmotic de-mineralized distilled water. The spray system is located upstream of the center of the test section in the straight section (9) before the convergence (8), and oscillates up and down to cover, when necessary, the entire test section height (1) (Figure 3). The super-cooled droplets impinge on the test model in the center of the test section. During a test, the water flows continually, the air pressure is open when the test begins, and the simulated cloud is formed in the IWT test section.
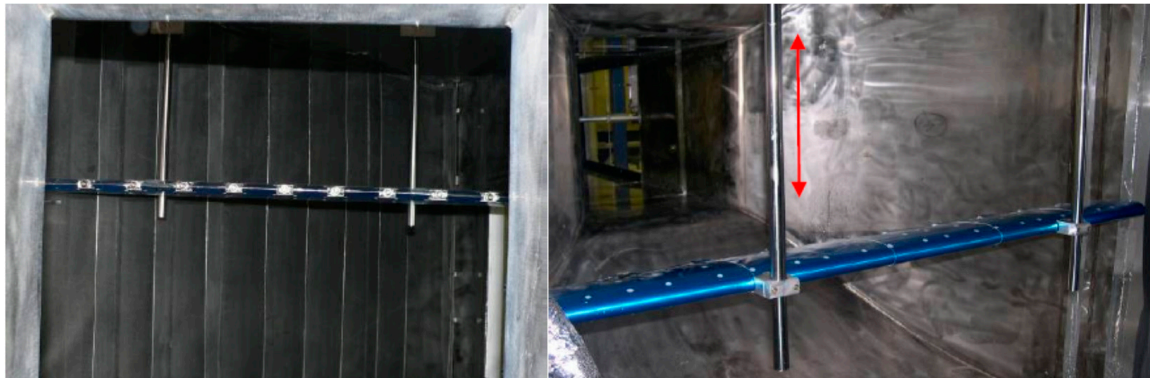
Figure 3. Sprinkler ramp.

Liquid Water Content Measurement and Droplet Median Volumetric Diameter

The liquid water content was calibrated at the beginning of the test series and measured using a LWC-200 liquid water content measuring device in the same manner as the King probe, in accordance with SAE ARP5905 [18]. The liquid water content is 0.8 g/m^3 with a standard deviation of 0.1 g/m^3, measured at the same height at which the blades are installed. At those settings, the droplet MVD generated in the tunnel is between 20 and 30 µm. Droplet MVD is measured with silicon oil, one of the techniques accepted and detailed in SAE AIR4906 [19].

2.2. Powered Spinning Rotor Blade Setup (P-SRB)

The powered spinning rotor blade (P-SRB) is a modification of the existing spinning rotor blade (SRB) setup developed at AMIL more than 10 years ago [3]. The original setup is composed of two blades in horizontal rotation connected to a hub and driven by a motor and a power shaft transmission. The SRB diameter, which is restricted by the AMIL IWT test section, is 0.780 m. The original setup is used to measure adhesion of representative atmospheric icing on different substrates, which can then be compared to bare aluminum or fiberglass blades to evaluate their ice Adhesion Reduction Factor (ARF). In the P-SRB (Figure 4), modifications were brought to the setup to bring electrical power to the spinning blades with the help of an IEC-FR-LC-10 Slipring by IEC Corporation, Sacramento CA, USA [20]. Power to supply the heating elements is generated by an EA-PS3150-04B laboratory power supply by Elektro-Automatik, Viersen, Germany.

(**a**)   (**b**)

Figure 4. P-SRB Setup (**a**) with aluminum and (**b**) with Coating 3.

2.2.1. Rotor Hub and Blades

The hub is connected to a 3600 RPM, 10 hp motor by a 2.54 cm (1″) diameter power steel shaft that is in turn connected to a 10 hp drive. For safety reasons, the maximum spinning speed was limited to 900 RPM. To safely operate the P-SRB in the IWT, the test section windows are made of polycarbonate thermoplastic resin (Lexan) which has a high impact resistance. The motor generator is computer-controlled and set at a constant rotor speed. The spinning rotor blade angular speed is measured by an optical encoder. The hub is a homemade modification of a G4 raptor hub with a diameter of 200 mm, as shown in Figure 5. This hub has no stabilizers. The blade pitch angle can be set at 0 and 6 degrees.
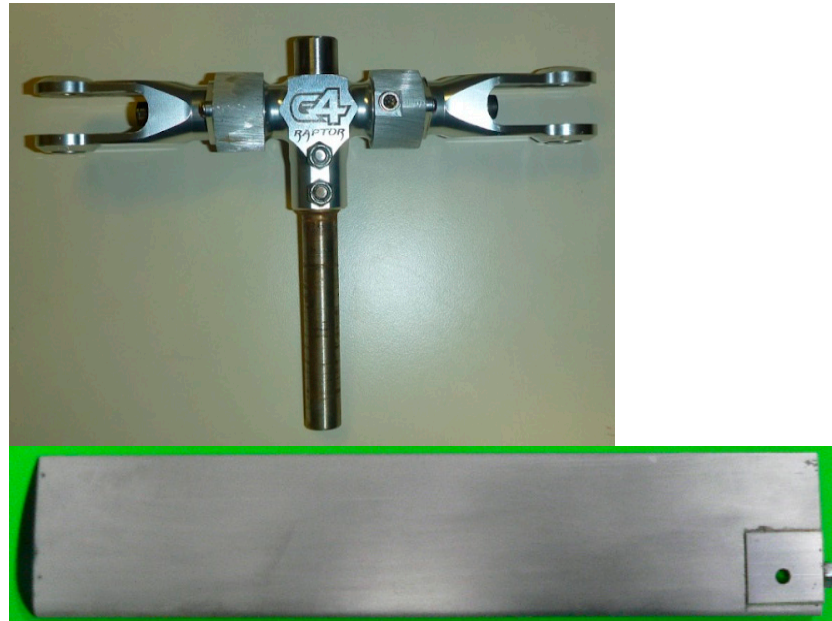

Figure 5. Rotor hub and blade.

The rotor blades are untwisted extruded 6063-T6 aluminum NACA0012 profiles used for tail rotor blades of small helicopters with a mill finish (Figure 6). The extruded rotor blade can easily be modified to suit the test requirements and were free of rivets or other imperfections. The blades characteristics are presented in Table 1. The span is the rotor blade length from the rotation point to the blade tip. The length is the blade length from the hand attachment to the blade tip (Figure 6).
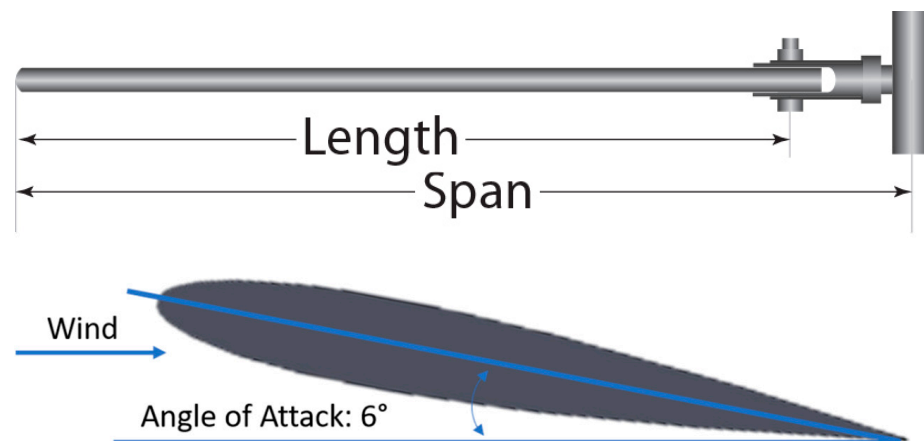

Figure 6. Blade length, span, and angle of attack (AOA).

Table 1. SRB blade characteristics.

| Blade Length	330	mm
Blade span (dia.)	780	mm
Blade chord	69.8	mm
Blade twist	0	deg
Blade pitch	6	deg
Blade number	2	
Airfoil	NACA0012	
Material	6063-T6 Al	

2.2.2. Measurements and Monitoring

A data acquisition system (DAS) is used to record data during each icing test. It is composed of a PCI-MIO16-XE-10 National Instrument card. The interface program was developed at AMIL to control the IWT and the SRB angular speeds and monitor the experimental data. The data monitored are the power consumed by the SRB measured at the drive exit, the main shaft speed obtained by an optical encoder, the SRB vibration measured at the support level with an accelerometer, as well as the IWT test section speed calculated from the pressure differential measured between the convergent entry and the test section. The temperature was measured in the test section with a type K thermocouple.

2.3. Heating Elements and RTDs

In this study, off the shelf heating element strips are used to represent a traditional electrothermal ice protection systems. The leading edge of the blades is covered with self-adhesive polyimide flexible heaters, 2.54×30.48 cm (1×12 in). The supplied voltage (U_V) and current (I_A) are varied according to each test. The total electric heating power is a direct result of the voltage and current variations. To help minimize losses and provide an even distribution of the heat, an aluminum tape is used to cover the heating element. The heating elements are used to protect the blade during icing tests in both anti-icing and de-icing modes.

Two RTDs are positioned on one of the blades to measure the temperatures at $r/R = 0.50$ and $r/R = 0.95$ (Figure 7). This blade is used to measure temperature whereas icing and ice shedding is observed on the second blade to prevent the RTDs to affect the results. Temperature is recorded at these different locations via a data logger at a rate of 5 recordings per second. The blade vibration rates were observed by the P-SRB interface program to guarantee stable rotation.
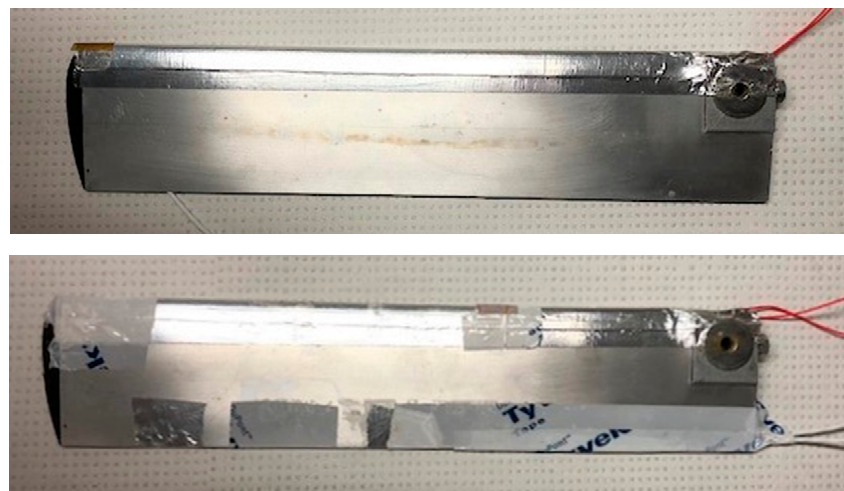
Figure 7. Aluminum blades with heating element and aluminum tape, with and without RTDs.

2.4. Surface Coatings

Innovative surface coatings are applied on the whole surface of the blades, over the heating elements, in order to measure their impact on the system performance and asses if they are worth using in a hybrid ice protection system to lower energy and power consumption. Four candidate coatings were tested in anti-icing and de-icing mode in the tunnel. According to the procedures stated by the suppliers, the coatings were sprayed onto the substrates and dried at room temperature for at least 48 h. For reasons of confidentiality, the names of the coatings will not be divulgated in this paper. However, different characteristics were measured and are presented in Table 2. The apparatus used for roughness measurements is a calibrated Surtronic 25 (Code #112-3522-10, serial #01-13-9009 made in UK, AMETEK Ultra Precision Technologies) from Taylor-Hobson®, Leicester, UK. Average roughness, expressed as Ra, is the mean value of measurements made directly on the substrate at three different directions. For wettability analysis, the water droplet contact angle (WCA) and contact angle hysteresis (CAH) were measured using a Kruss™ (Hamburg, Germany) DSA100 goniometer at 25 ± 0.5 °C. A 5 μL water droplet was placed on the surface to evaluate the WCA by Young–Laplace approximation. By moving the needle tip within the water droplet, the CAH was determined as the difference between advancing and receding contact angles. The adhesion reduction factor (ARF) represents the ratio of the ice adhesion on bare aluminum with the ice adhesion on the coating. This value has been measured with the centrifuge adhesion test (CAT) detailed in [21] and [22]. Coatings 1 and 4 are silicone and siloxane based commercially available superhydrophobic coatings, while Coating 3 is a commercially available hydrophobic coating (lower contact angle). Coating 2 is a hydrophobic epoxy-based coating, highly mechanically resistant. All the blades covered with the different coatings are shown at Figure 8. With ARFs below 10, the coatings are not considered, or only slightly, icephobic. For Coating 4, the ARF could not be measured since the coating was not available at the time of that measurement. However, the coating is not characterized as icephobic by the manufacturer.

Table 2. Substrate characteristics.

Substrate	Roughness Ra (μm)	WCA (°)	CAH (°)	ARF CAT
Aluminum	0.8	93	34	1
Coating 1	5.0	153	4	3.6
Coating 2	2.0	110	35	6
Coating 3	3.9	112	10	6.8
Coating 4	4.9	152	9	N/A

(a)   (b)   (c)   (d)
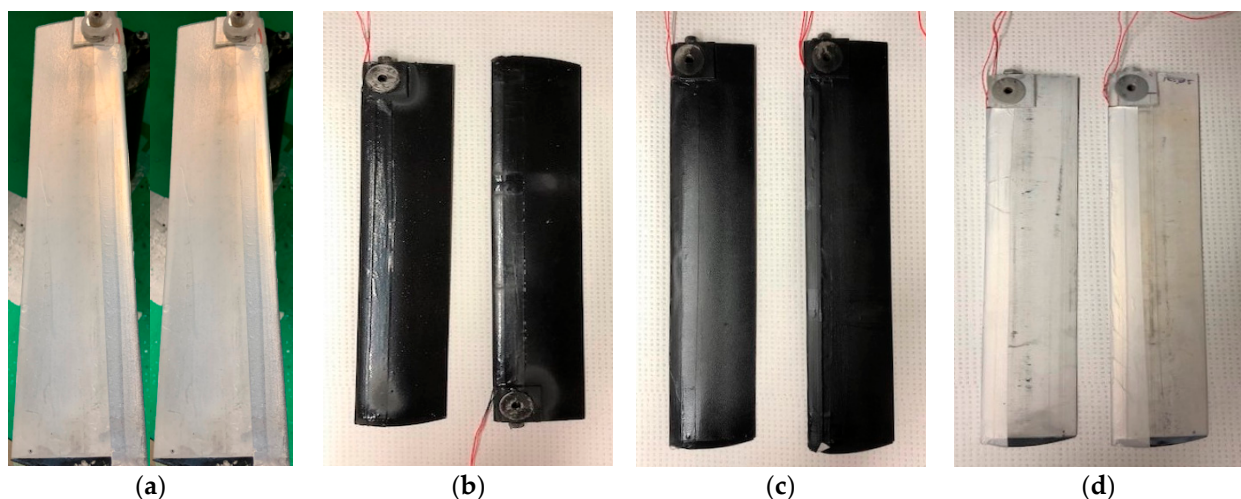
Figure 8. Blades covered with (**a**) Coating 1; (**b**) Coating 2; (**c**) Coating 3; and (**d**) Coating 4.

2.5. Test Conditions

The test conditions are presented at Table 3. Tests are performed in Anti-icing and in de-icing modes, which are described in the results section. Tests are performed at two air temperatures: $-15\,°C$ and $-7.5\,°C$ in order to obtain two different types of ice (mixed, a combination of clear and rime ice, and glaze ice respectively).

Table 3. Test conditions.

Test Mode	$T_\propto$ (°C)	V_∞ (m/s)	V Angular (RPM)	LWC (g/m^3)	MVD (µm)	θ (°)
Anti-icing	−15 −7.5	30	900	0.8	20 to 30	6
De-icing	−15 −7.5					

3. Results

This section presents the different results obtained during experimentation with the bare aluminum blades and with the blades covered with the four different coatings. Results are separated in two different sections, one for the test performed under an anti-icing mode and one for those performed under a de-icing mode. In anti-icing mode, power supplied to the blade is gradually lowered until traces of ice starts to appear on the whole leading edge while in de-icing mode, an ice layer is first accreted and power supplied to the elements is gradually increased until ice shedding is obtained from the test blade. Problems were encountered with the signals from the RTDs and temperature measurements could not be done for these series of testing. Signals received from the slip ring was intermittent and would suddenly vary significantly to inconsistent values. Troubleshooting has to be done to fully understand the problematic and correct it before a next test campaign.

3.1. Anti-Icing

This section presents the results obtained in Anti-icing mode. During those tests, the blades are put in rotation in the wind tunnel. Maximum power is then supplied to the blade in order to ensure no ice accumulation on the blade. Water spraying is then initiated in the tunnel and then power is decreased gradually until ice is accreted on the whole leading edge of the blade. During this process, the power is recorded at four important steps: (1) when runback water appears on top of the blade and (2) at the bottom of the blade, (3) when ice is first witnessed at the tip of the blade, and (4) when the leading edge is first entirely covered with ice (complete radius). As opposed to de-icing, in anti-icing usually no ice accretes on the blades. Those steps represent the different accumulation that can occur on the blade which all need to be prevented and the power measured show the minimum power to prevent that particular accumulation. Separating the tests this way helps highlight the different power required for each accumulation as well as the different ways a coating can help reduce total power consumption, (for example: when preventing runback accumulation). Figure 9 shows pictures of steps 1–4 taken with a video camera during testing. The steps are defined in the order they are expected to be encountered most of the time (based on experiences), but the order and/or occurrence of the steps can vary depending on the test and coating behaviors.

3.1.1. Air Temperature of $-7.5\,°C$

All the coatings are first tested at an ambient air temperature of $-7.5\,°C$ in the wind tunnel. At this air temperature with the other test conditions selected (LWC, MVD, RPM, etc.), the ice accretion obtained is a glaze ice, as shown under Section 3.2.1. Three test repetitions are performed with each substrate. Figure 10 presents the power density for the different substrate at steps 1 to 4 during testing that is calculated by dividing the total power consumption by the surface area of the heating elements ($2 \times 1 \times 12$ in^2).
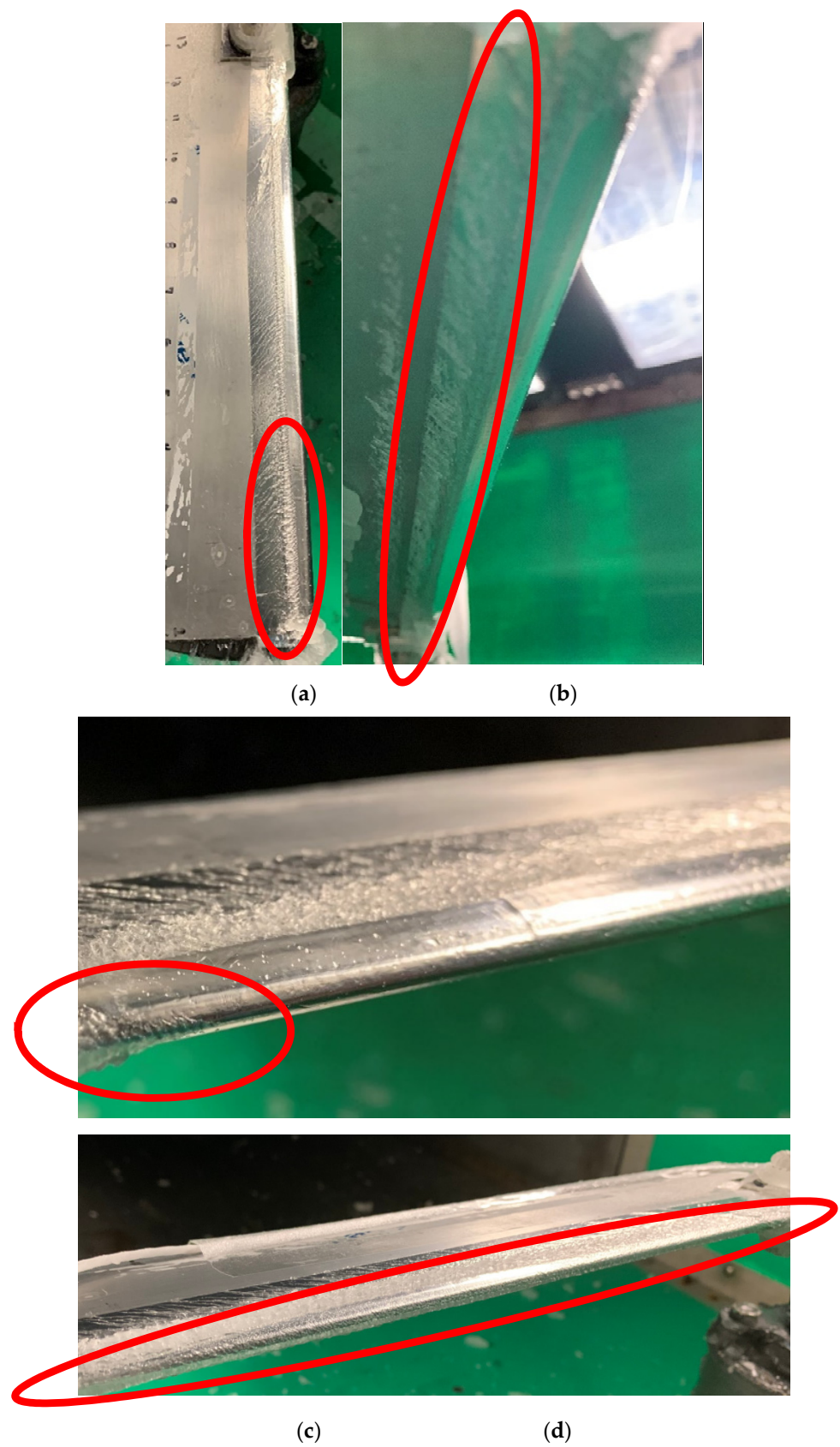
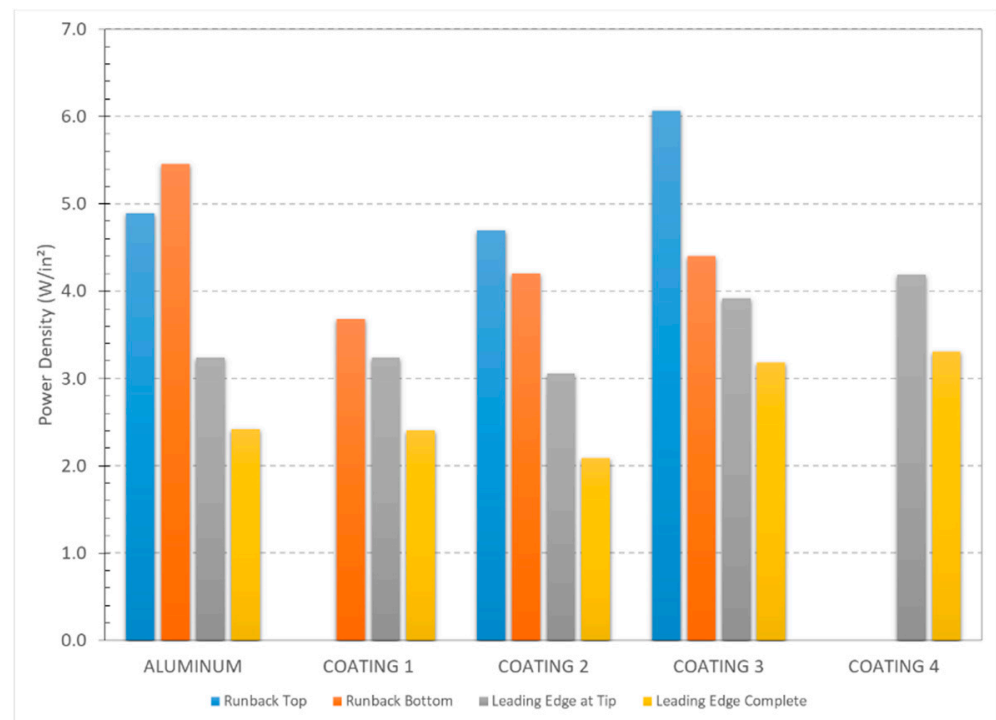**Figure 9.** Pictures of (**a**) step 1; (**b**) step 2; (**c**) step 3; and (**d**) step 4 during anti-icing tests on aluminum.

Figure 10. Power density obtained during anti-icing tests at -7.5 °C measured when ice accretion is first initiated at different positions on the blade.

For the case of runback on the top of the blade, the power and power density are 118 ± 7 W and 4.9 ± 0.3 W/in^2 for the Aluminum, 113 ± 11 W and 4.7 ± 0.5 W/in^2 for Coating 2, 145.6 ± 27 W and 6.1 ± 1.1 W/in^2 for Coating 3 while no runback is obtained with Coatings 1 and 4.

For runback on the bottom, the power and power density are 131 ± 8 W and 5.5 ± 0.4 W/in^2 for Aluminum, 88 ± 7 W and 3.7 ± 0.3 W/in^2 for Coating 1, 101 ± 20 W/in^2 and 4.2 ± 0.8 W/in^2 for Coating 2, 105.7 ± 23 W/in^2 and 4.4 ± 1.0 W/in^2 for Coating 3, and no runback for Coating 4.

For the initiation of the ice accumulation on the leading edge at the tip of blade, the power and power density are 78 ± 8 W and 3.2 ± 0.4 W/in^2 for the aluminum, 78 ± 1 W and 3.2 ± 0.1 W/in^2 for Coating 1, 73 ± 6 W and 3.1 ± 0.3 W/in^2 for Coating 2, 94.1 ± 12 W and 3.9 ± 0.5 W/in^2 for Coating 3, and 100 ± 1 W and 4.2 ± 0.1 W/in^2 for Coating 4.

Finally, for an ice accumulation on the whole leading edge, the power and power density are 58 ± 9 W and 2.4 ± 0.4 W/in^2 for the aluminum, 58 ± 2 W and 2.4 ± 0.1 W/in^2 for Coating 1, 50 ± 9 W and 2.1 ± 0.4 W/in^2 for Coating 2, 76.3 ± 5 W and 3.2 ± 0.2 W/in^2 for Coating 3, and 79 ± 4 and 3.3 ± 0.1 W/in^2 for Coating 4.

The results show a diminution of the power between each step except for the aluminum between steps 1 and 2, where runback first accreted at the bottom of the blade. For Coating 1, no runback was obtained on the top of the blade during the whole test, while for Coating 4 no runback accumulated on the blade at all, only at the leading edge (Figure 11). For the ice accumulation on the leading edge, only Coating 2 shows a reduction in power consumption as compared to aluminum, while the other coatings all increased the power required to maintain the leading edge free of ice.
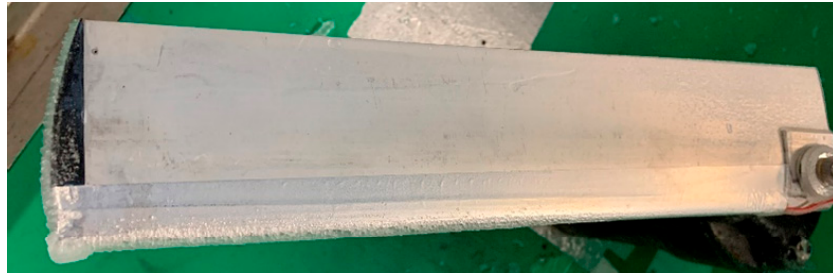
Figure 11. Pictures of the runback free blade (only ice accretion on the leading edge) with Coating 4.

3.1.2. Air Temperature of $-15\,^{\circ}$C

Testing is repeated with the same test procedure but with an ambient air temperature of $-15\,^{\circ}$C. Due to time limitation only aluminum and Coating 2 were tested. Coating 2 is selected since it is the only coating that showed a power reduction for the accumulation on the leading edge. Testing is repeated three times for each of the two substrates. At this temperature and other test conditions selected, ice accretion obtained was a mixed ice, a combination of clear and rime ice (see Section 3.2.2).

Figure 12 presents the power density consumed for the aluminum and Coating 2 at steps 1 to 4. For Runback on the top of the blade, the power and power density are 247 ± 21 W and 10.3 ± 0.9 W/in^2 for the aluminum and 138 ± 16 W and 5.7 ± 0.7 W/in^2 for Coating 2. For runback on the bottom, the power and power density are 218 ± 12 W and 9.1 ± 0.5 W/in^2 for aluminum and 173 ± 16 W/in^2 and 7.2 ± 0.7 W/in^2 for Coating 2. For the initiation of the ice accumulation on the leading edge at the tip of the blade, the power and power density are 123 ± 1 W and 5.1 ± 0.1 W/in^2 for the aluminum and 151 ± 35 W and 6.3 ± 1.5 W/in^2 for Coating 2. Finally, for an ice accumulation on the whole leading edge, the power and power density are 112 ± 8 W and 4.7 ± 0.3 W/in^2 for the aluminum and 120 ± 12 W and 5.0 ± 0.5 W/in^2 for Coating 2.

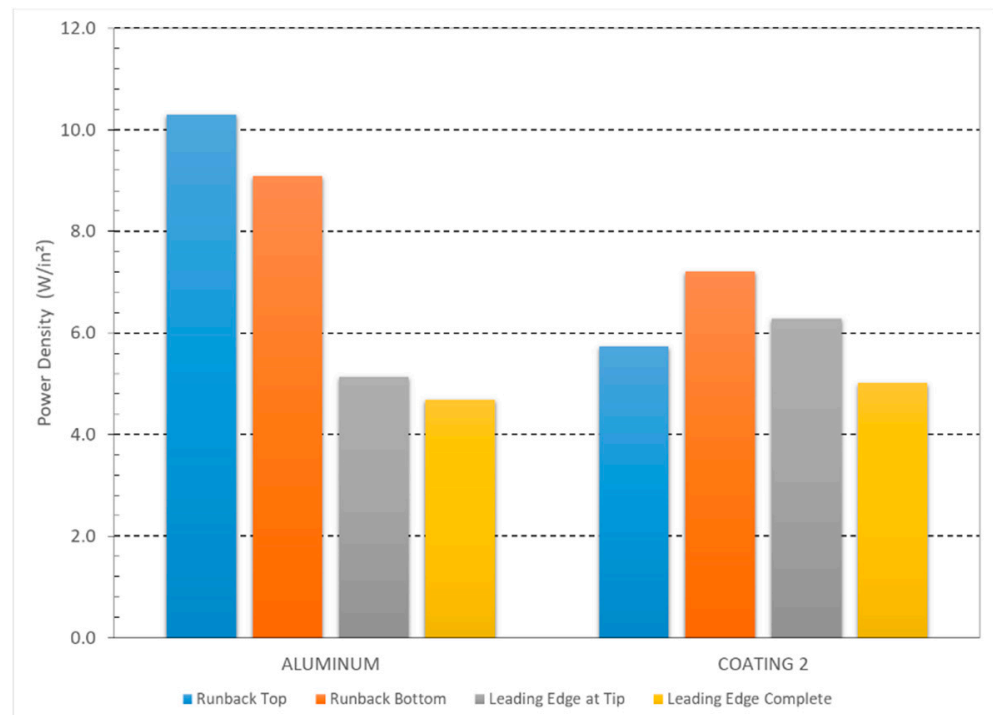**Figure 12.** Power density obtained during anti-icing tests at $-15\,^{\circ}$C measured when ice accretion is first initiated at different positions on the blade.

As opposed to the results at −7.5 °C, a decrease of the power between each step is obtained for the aluminum but not between steps 1 and 2, where runback first accreted at the bottom of the blade, for Coating 2. Also, Coating 2 does not allow a power consumption reduction when compared to aluminum at this temperature.

3.2. De-Icing

In this section, the results obtained under a de-icing regime are presented. For those tests, blades are put in rotation in the wind tunnel and the air temperature is stabilized. Then, the icing cloud is generated in the test section and ice starts accumulating on the rotating blade. Icing in the tunnel is stopped when an ice thickness of 6 mm is obtained at the tip of the blade, which corresponds to the maximum thickness allowed on the main rotor blades of a rotorcraft studied in this project. To obtain the desired ice thickness, accumulation is done on the rotating blades prior to testing and the ice thickness is measured with a caliper. The time to reach the desired thickness is recorded and used to define the icing time for the different tests at each condition. This process was repeated multiple times at each single condition to ensure that the method provides repeatable ice thicknesses and the resulting thickness only varied by less than 0.6 mm, which was considered acceptable. After the ice accumulation, minimum power is supplied to the heating elements and gradually increased until shedding the ice layer from the test blade. Ice shedding is detected by the sound of the ice impacting on the tunnel walls and by a significant vibration spike measured by an accelerometer installed on the setup for vibration surveillance. Shedding is when ice the complete ice layer accreted on the leading edge detaches from the blade, besides the small residual part at the root of the blade. Power is recorded throughout the test.

3.2.1. Air Temperature of −7.5 °C

As for the tests in Anti-icing mode, testing is performed with bare aluminum blades and with the four different coatings at −7.5 °C. Ice accumulation obtained is, again, for those test conditions a glaze ice accumulation. Ice thickness varies along the radius of the blade due to the tangential velocity increase with the radial position. Resulting ice accumulation is shown at Figure 13.

Figure 13. Glaze ice accumulation on aluminum during de-icing tests at −7.5 °C.

Testing is repeated three times for each substrate and the average power density obtained for all the different substrates is presented in Figure 14. The total power consumption for the aluminum is 95.1 ± 2.0 W with a power density of 4.0 ± 0.1 W/in^2, while it is 104.3 ± 8.2 W with a power density of 4.3 ± 0.3 W/in^2 for Coating 1, 93.3 ± 9.6 W with a power density of 3.9 ± 0.4 W/in^2 for Coating 2, 92.4 ± 11.6 W with a power density of 3.9 ± 0.5 W/in^2 for Coating 3 and 113.9 ± 12.8 W with a power density of 4.7 ± 0.5 W/in^2 for Coating 4. A small reduction in power as compared to aluminum is obtained for Coatings 2 and 3. However, when looking at the three test repetitions for Coating 3, it can be observed that the coating suffers degradation throughout testing. The first result

obtained is 79.5 W, significantly lower than aluminum, while for the second and third test the power consumption increases to 95.9 and 101.8 W, which is higher than the case of bare aluminum.
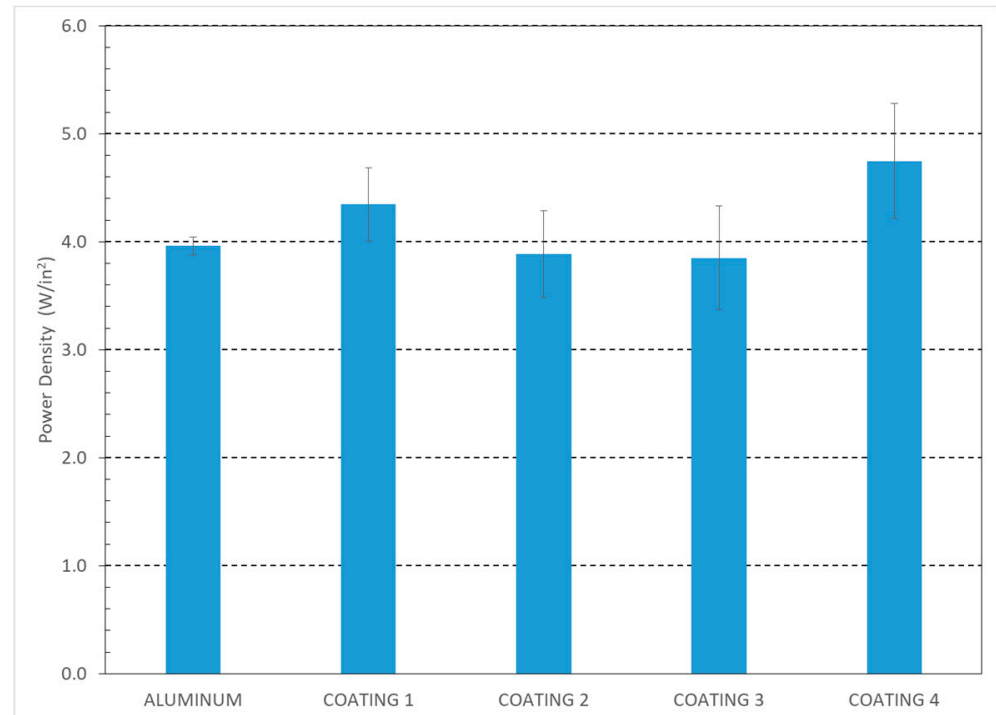

Figure 14. Power density at ice shedding obtained during anti-icing tests at -7.5 $°C$.

3.2.2. Air Temperature of -15 $°C$

Testing is also performed at -15 $°C$ but due to time restriction, only bare aluminum and Coating 2 are tested. Coating 3 is not tested because of the resulting degradation from testing at -7.5 $°C$. The ice accumulation obtained is a mixed ice which is a combination of clear and rime ice (Figure 15). Three test repetitions are performed with each substrate and the power densities obtained are presented at Figure 16. For the aluminum the power is 188.6 ± 6.0 W with a power density of 7.9 ± 0.3 W/in^2. For Coating 2, the power consumption and density are higher than for aluminum with values of 205.0 ± 8.5 W and 8.5 ± 0.4 W/in^2, respectively.

Figure 15. Mixed ice accumulation, a combination of clear and rime ice, on aluminum during de-icing tests at -15 $°C$.
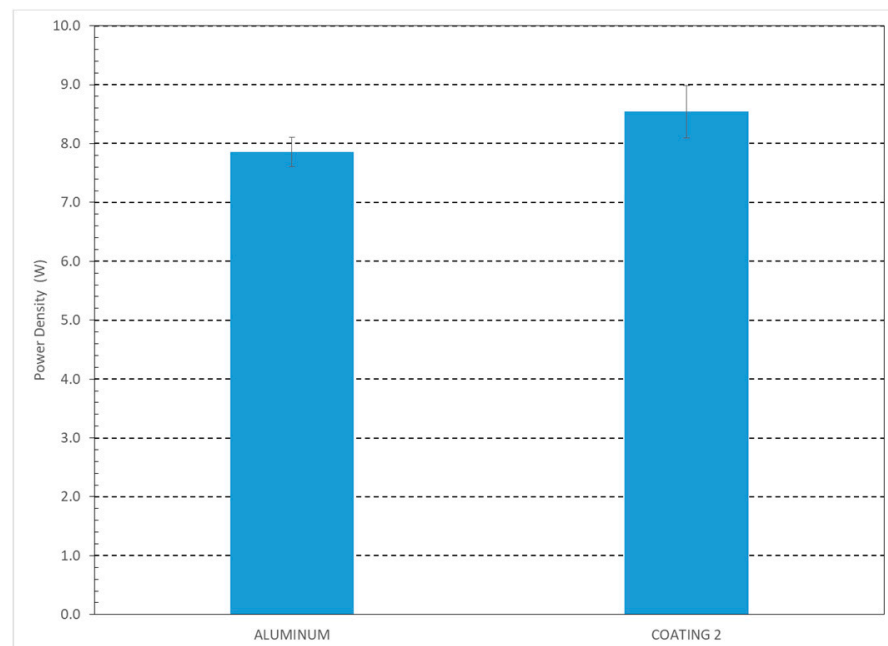
Figure 16. Power density at ice shedding obtained during anti-icing tests at −15 °C.

4. Discussion

In this section, the impact of the coatings on an electrothermal ice protection system, whether working in anti-icing or in de-icing mode, is analyzed when compared to bare aluminum blades.

4.1. Anti-Icing Mode

The power difference for each step between the coatings and the bare aluminum blades are presented at Table 4. Besides Coating 2 at −7.5 °C, the coatings either increased the power required to protect the leading edge of the blade or had no effect. At −15 °C, Coating 2 did not improve the system's performance and the power was as high as for the other coatings at −7.5 °C. This power increase could be attributed to the additional insulation that the coating layer brings between the surface and the heating element. This coating is epoxy based and epoxy is known to be a good insulator, being more than 1000 times less thermally conductive than aluminum. It would be interesting to measure this insulation and determine a correlation between these results and the added insulation. This conclusion signifies that once insufficient power is supplied to prevent nucleation of the water droplets at impact on the leading edge, the coatings tested have no positive impact on the system. This is in accordance with the accumulation obtained at the leading edge and the ice accumulation obtained in de-icing mode. As detailed in the next section (Section 4.2), the ice accumulates at a similar rate when no power is supplied in de-icing mode and the resulting accumulation is similar on all substrates, showing that the coatings tested have no effect on ice accumulation.

On the other hand, the coatings tested significantly affected the runback effect on the blades. Except for the runback on the top of the blade with Coating 3, all the coatings reduced the power by up to 44% before runback started accumulating. For Coating 4, no runback was at all accumulated for the three test repetitions performed; while for Coating 1, no runback accumulated on the top of the blade. This means that when the power is sufficient to prevent freezing of the droplets and allow flow off from the leading edge, the hydrophobic nature of the coatings tested facilitate water flow off from the blade. The superhydrophobic coatings (1 and 4) even completely prevent runback accumulation on the blade (upper surface only for Coating 1). This can lead to a significant positive effect on an ice protection system in anti-icing mode. For example, if Coating 4 is applied, instead of having to supply more than 131 W to prevent any ice accumulation, including no runback,

on the blade, only around 100 W are required, which is a power reduction of 24% of the power consumed by the system. If Coating 4 could be applied on the leading edge only (resulting in no added insulation over the heating elements) and still provide the same benefit of better water flow off (which is plausible but has yet to be demonstrated) the power could be reduced to 78 W. This represents a power reduction of 40% which is very significant for such systems, considering the limited power available on a rotorcraft.

Table 4. Anti-icing power reduction compared to aluminum due to presence of coating.

T_∞ (°C)	Test Step	Coating 1	Coating 2	Coating 3	Coating 4
−15	Runback top	N/A	−44%	N/A	N/A
	Runback bottom	N/A	−21%	N/A	N/A
	Leading edge and tip	N/A	+23%	N/A	N/A
	Leading edge complete	N/A	+7%	N/A	N/A
−7.5	Runback top	-	−5%	+24%	-
	Runback bottom	−33%	−23%	−19%	-
	Leading edge and tip	0%	−7%	+21%	+28%
	Leading edge complete	0%	−14%	+31%	+36%

4.2. De-Icing Mode

In de-icing mode, an ice layer is first accumulated on the blades before power is supplied to the heating elements. As mentioned in the previous section, the accumulation rate is similar for all substrates and increases linearly with the radius. Also, the type of ice accumulation is the same on all substrates and resulting accumulations do not show any difference for any substrate. This tends to confirm the conclusion obtained in anti-icing mode that the coatings tested do not provide any benefit when the power is not sufficient to prevent water droplets impinging from freezing on the leading edge.

The power difference to generate ice shedding from the blade as required by the coatings and compared to bare aluminum blades is presented at Table 5. The results show that the presence of the coatings tested has a very minor effect on the power required for ice shedding from the blade. Coating 4 increases the power required by 20%, while all other surfaces impact the power by less than 10%, which is close to the experimental variability. The coatings tested were not—or very slightly—icephobic, as shown by their ARF values (Table 2), meaning that they do not significantly reduce the adhesion of the ice. This can explain this slight effect on the power consumption at shedding. It would be interesting to pursue testing on coatings showing high icephobicity. Also, a small zone at the root of the blade exists where there is no wire in the heating element resulting in no heating. At this position, the ice stays anchored to the blade and a cohesive break has to occur within the ice layer for ice shedding. A short part of the ice layer remains on the blade as shown at Figure 17. This is expected to have an influence on the results obtained, which could be part of the reasons for the uniform results for all the substrates. These preliminary experiments have allowed to observe this phenomenon and will allow further improvement of the setup. By improving the setup, it will be possible to quantify this effect and increase the fidelity of the results.

Table 5. De-icing power reduction compared to aluminum due to presence of coating

Test Mode	T_∞ (°C)	Coating 1	Coating 2	Coating 3	Coating 4
De-Icing	−15	N/A	+9%	N/A	N/A
	−7.5	+10%	−2%	−3%	+20%

Figure 17. Short layer of ice remaining on the blade after ice shedding during de-icing tests.

5. Conclusions

This paper presents the design and development of a new test setup to perform experimental testing of different powered ice protection systems on rotating blades. By modifying an existing setup at the laboratory, it was possible to bring electric power to the rotating blades in a wind tunnel submitted to different representative atmospheric icing clouds. After the completion of the setup, preliminary testing was done to test the new apparatus. An electrothermal ice protection system was tested at two temperatures and compared with a hybrid version of the same system where hydrophobic/superhydrophobic coatings were applied at the surface with the hope of reducing power consumption due to the water repellant properties of the coatings. This made it possible to measure their impact on the system performance when compared to the standard system. Tests were performed in both anti-icing and in de-icing mode.

In anti-icing, the coatings tested did not show any improvement on the power consumption to keep the leading edge of the blade, where the ice accumulation occurs, free of ice. On the other hand, all the coatings tested reduced the power required to keep the blade completely clean without any runback ice accumulation. One of the coatings totally prevented runback accumulation. That coating could reduce power consumption in anti-icing by up to 44% if only applied away of the leading edge and on the rest of the blade, which is significant with the limited power available on rotorcraft. This showed that the coatings tested had no positive effect when the droplet freezes at impact on the leading edge, but were effective when the droplets were kept in a liquid form and could flow off the leading edge favoring their flow off from the blade.

In de-icing, the results were similar for all the substrate tested, including for the bare aluminum blades. The low icephobicity of the coatings tested could explain this result. Testing with highly icephobic coatings should be done to see if a more significant impact could be obtained with such coatings. It was observed that, due to a small unheated zone at the root of the blade, a short part of the ice accumulation did not shed from the blade increasing the force required for ice shedding to generate the cohesive break in the ice layer itself. Improvements must be made to the setup to prevent this effect and increase the accuracy of the results. Also, additional camera systems—including thermal and IR cameras—will be mounted on the wind tunnel for better imaging of the tests. Preliminary investigation with one thermal and/or IR camera will be done first to assess the advantages of using such a device, and if the results are positive, a complete camera system which could include multiple thermal/IR cameras mixed with standard video cameras will be designed to optimize visualization of the different processes involved at different key angles.

The developed setup proves successful for the testing of an electrothermal ice protection system in anti-icing mode; while in de-icing mode slight improvements must be made to increase their accuracy. The improvements are minor and the results are still deemed reliable and repeatable even for preliminary experiments, with an experimental variability below 15% for the tests on bare aluminum. With this successful proof-of-concept, this new experimental test setup will allow the design, testing, and characterization of different ice protection systems for small scale tests under representative atmospheric icing. The next step, after making the improvements required, will be to test a mechanically operated-icing system for rotorcraft, which will be presented in a future publication.

References

1. Brouwers, E.W.; Palacios, J.L.; Smith, E.C.; Peterson, A.A. The experimental Investigation of a Rotor Hover Icing Model with Shedding. In *The American Helicopter Society 66th Annual Forum*; American Helicopter Society: Phoenix, AZ, USA, 2010.
2. Fortin, G.; Perron, J. Wind Turbine Icing and De-icing. In Proceedings of the 47th Aerospace Science Meeting and Exhibit, Orlando, FL, USA, 5–8 January 2009.
3. Fortin, G.; Perron, J. Spinning Rotor Blade Tests in Icing Wind Tunnel. In Proceedings of the 1st AIAA Atmospheric and Space Environments Conference, San Antonio, TX, USA, 22–25 June 2009; pp. 1–16.
4. Wang, Z.; Zhu, C.; Zhao, N. Experimental Study on the Effect of Different Parameters on Rotor Blade Icing in a Cold Chamber. *Appl. Sci.* **2020**, *10*, 5884. [CrossRef]
5. Liu, Y.; Li, L.; Ning, Z.; Tian, W.; Hu, H. Experimental investigation on the dynamic icing process over a rotating propeller model. *J. Propuls. Power* **2018**, *34*, 933–946. [CrossRef]
6. Oleskiw, M.; Hyde, F.; Penna, P. In-flight icing simulation capabilities of NRC's altitude icing wind tunnel. In Proceedings of the 39th Aerospace Sciences Meeting and Exhibit, Reno, NV, USA, 8–11 January 2001.
7. Orchard, D.; Chevrette, G.; Maillard, D.; Khoun, L. Testing of elastomer icephobic coatings in the AIWT: Lessons learned. *SAE Int. J. Adv. Curr. Pract. Mobil.* **2019**, *2*, 238–244.
8. Laroche, A. Comparative Evaluation of Embedded Heating Elements as Electrothermal Ice Protection Systems for Composite Structures. Ph.D. Thesis, Concordia University, Montréal, QC, Canada, 2017.
9. Antonini, C.; Innocenti, M.; Horn, T.; Marengo, M.; Amirfazli, A. Understanding the effect of superhydrophobic coatings on energy reduction in anti-icing systems. *Cold Reg. Sci. Technol.* **2011**, *67*, 58–67. [CrossRef]
10. Drury, M.D.; Szefi, J.T.; Palacios, J.L. Full-scale testing of a centrifugally powered pneumatic de-icing system for helicopter rotor blades. *J. Aircr.* **2017**, *54*, 220–228. [CrossRef]
11. Palacios, J.; Wolfe, D.; Bailey, M.; Szefi, J. Ice testing of a centrifugally powered pneumatic deicing system for helicopter rotor blades. *J. Am. Helicopter Soc.* **2015**, *60*, 1–12. [CrossRef]
12. Palacios, J.L.; Han, Y.; Brouwers, E.W.; Smith, E.C. Icing environment rotor test stand liquid water content measurement procedures and ice shape correlation. *J. Am. Helicopter Soc.* **2012**, *57*, 29–40. [CrossRef]
13. Palacios, J.L. Design, fabrication, and testing of an ultrasonic de-icing system for helicopter rotor blades. In *Department of Aerospace Engineering*; The Pennsylvania State University: State College, PA, USA, 2008; p. 205.
14. Li, L. Experimental investigations on ice accretion process and anti-/de-icing technology for aero-engine icing mitigation. In *Aerospace Engineering*; Iowa State University: Ames, IA, USA, 2018; p. 142.
15. Huang, X.; Tepylo, N.; Pommier-Budinger, V.; Budinger, M.; Bonaccurso, E.; Villedieu, P.; Bennani, L. A survey of icephobic coatings and their potential use in a hybrid coating/active ice protection system for aerospace applications. *Prog. Aerosp. Sci.* **2019**, *105*, 74–97. [CrossRef]
16. Samad, A.; Villeneuve, E.; Morency, F.; Volat, C. A numerical and experimental investigation of the convective heat transfer on a small helicopter rotor test setup. *Aerospace* **2021**, *8*, 53. [CrossRef]

17. Villeneuve, E.; Perron, J. *Icing Wind Tunnel Certification Tests in Accordance with SAE ARP5905 and AIR4906*; AMIL: Chicoutimi, QC, Canada, 2012; p. 80.
18. SAE International ARP5905. *Calibration and Acceptance of Icing Wind Tunnels*; SAE International: Warrendale, PA, USA, 2003.
19. SAE International AIR4906. *Droplet Size Instrumentation Used in Icing Facilities*; SAE International: Warrendale, PA, USA, 1995.
20. IEC Corporation Slip Ring Assemblies. Flange Mount Slip Ring. 2020. Available online: https://ieccorporation.com/flange-mount/ (accessed on 23 December 2020).
21. Brassard, J.D.; Laforte, C.; Guerin, F.; Blackburn, C. *Icephobicity: Definition and Measurement Regarding Atmospheric Icing*; Springer: Berlin/Heidelberg, Germany, 2017; pp. 1–21.
22. Laforte, C.; Blackburn, C.; Perron, J. A Review of Icephobic Coating Performances over the Last Decade, 2015-01-2149. In *Conference on Icing of Aircraft, Engines, and Structures*; SAE International: Prague, Czech Republic, 2015.